chemosensors

Article

Pneumatic Cell Stretching Chip to Generate Uniaxial Strain Using an Elastomeric Membrane with Ridge Structure

Xu Fang [1], Pudi Wang [2], Feng Lin [3,*], Jianyong Huang [2], Jing Fang [2] and Chunyang Xiong [1,2,3,*]

[1] Academy for Advanced Interdisciplinary Studies, Peking University, Beijing 100871, China; 1701111434@pku.edu.cn
[2] Department of Mechanics and Engineering Science, College of Engineering, Peking University, Beijing 100871, China; pd_wang@pku.edu.cn (P.W.); jyhuang@pku.edu.cn (J.H.); jfang@pku.edu.cn (J.F.)
[3] Wenzhou Institute, University of Chinese Academy of Sciences, Wenzhou 325000, China
* Correspondence: linfeng@ucas.ac.cn (F.L.); cyxiong@pku.edu.cn (C.X.)

Abstract: Cyclic mechanical stretching, including uniaxial strain, has been manifested to regulate the cell morphology and functions directly. In recent years, many techniques have been developed to apply cyclic mechanical stretching to cells in vitro. Pneumatically actuated stretching is one of the extensively used methods owing to its advantages of integration, miniaturization, and long-term stretching. However, the intrinsic difficulty in fabrication and adjusting the strain mode also impedes its development and application. In this study, inspired by the topological defects principle, we incorporated a ridge structure into the membrane surface of a traditional pneumatic cavity stretching chip to regulate the strain mode. Our results showed that the surface ridge structure can directly change the equiaxial stretching mode to the standard uniaxial strain, and it is ridge width-independent. The uniaxial strain mode was further proved by the cell orientation behavior under cyclic stretching stimulation. Moreover, it is easy to realize the multimodal strain fields by controlling the width and height of the ridge and to achieve high-throughput testing by creating a cavity array using microfabrication. Together, we propose a smart method to change the surface strain field and introduce a simple, yet effective, high-throughput pneumatically actuated uniaxial stretching platform, which can not only realize the multimodal mechanical stimulation but also achieve multiscale mechanosensing behaviors of single-cell or multi-cell (tissue and/or organoid) mechanobiology applications.

Keywords: pneumatic cell stretching chip; ridge structure; uniaxial strain; cell orientation; cell mechanosensing

Citation: Fang, X.; Wang, P.; Lin, F.; Huang, J.; Fang, J.; Xiong, C. Pneumatic Cell Stretching Chip to Generate Uniaxial Strain Using an Elastomeric Membrane with Ridge Structure. *Chemosensors* **2022**, *10*, 302. https://doi.org/10.3390/chemosensors10080302

Academic Editors: Chunsheng Wu and Christos Kokkinos

Received: 28 June 2022
Accepted: 27 July 2022
Published: 1 August 2022

1. Introduction

Cells live in complex biochemical and biophysical microenvironments, including mechanical stimulations [1,2]. Recently, numerous researchers have suggested that mechanical stimulations, especially mechanical stretching, play an important role in regulating many cellular biological activities, such as proliferation, apoptosis, differentiation, and migration [3–8]. In the human body, cyclic mechanical stretching participates in many biological activities, such as vasodilator [9–11], peristaltic of intestines [9,12], alveoli ventilation function [13,14], and the activity of muscle fibers [6,15]. Uniaxial stretching, as a major mode of mechanical stretching, has been widely accepted as the common cyclic mechanical stretching mode for the investigation of a cell function and behavior in response to mechanical stimulation due to its explicit stretching mode and robust post-analysis strategy.

To implement uniaxial stretching, many integrated and interesting devices have been developed [1,2,8,16–19]. These devices can be mainly classified into three types based on the actuating principle: servomotor-actuated device, magnetically actuated device, and pneumatically actuated device. Servomotor-actuated devices are often integrated with an external stepper motor that pulls the elastomeric membrane in one direction to realize

uniaxial stretching [18,19]. Although this kind of device can precisely control the accuracy of stretching, the overheating of the external motor system impedes its long-term stimulation application. Additionally, these devices generally fail to realize stretching at different strain levels simultaneously, which hinders increasing the experiment throughput. A magnetically actuated system is another commonly used method to apply uniaxial stretching [20,21]. The device is integrated with magnetic materials as the magnetic pole. When this device is exerted under a magnetic field, uniaxial stretching occurs in the direction of the magnetic field. Although this technology can realize long-term stretching, the device size results in low-throughput and poor integration. Compared to these methods, the pneumatic actuation manner has outstanding advantages of high-throughput, versatility, and long-term stretching. Typically, there is a commercial pneumatically actuated cell stretching device, i.e., Flexcell.

Another most accepted pneumatically actuated layout is a balloon-like device in which positive air pressure is loaded to stretch the elastic membrane on a circle cavity [15,17,22,23]. This kind of device can easily obtain a uniform equiaxial stretch mode, high-throughput, and long-term stretching by integrating the microfluidic platform. However, these devices fail to apply the well-accepted uniaxial stretching mode due to intrinsic structure limitations. Although some strategies have been proposed to solve this problem through designing double- or three-layer structure devices in which a vacuum is obtained in the by-side channels [6,19,22–24]. Those multilayer structure devices need complex fabrication and careful alignment of the multilayer structure [11,25–27]. The fatal flaw of the multilayer structure device is a poor alignment performance of elastic posts between the membrane, causing poor stretching. Thus, it is necessary to come up a new, simple, effective, long-term, and high-throughput device, which not only applies a well-accepted uniaxial stretch stimulation but also overcomes these drawbacks of the commonly used method.

Herein, inspired by the topological defects principle, we sought to introduce a periodic ridge structure to the pneumatically actuated balloon-like device to produce uniaxial stretching, which was validated by a FEM simulation and experimental method, including the cell orientation response, and further determine how the geometric parameters of the ridge could dictate the strain field. We found that the strain manner can be easily changed by introducing the ridge structure into the traditional pneumatically actuated balloon-like device, which generated a uniaxial strain. Moreover, it is easy to realize multimodal strain fields by controlling the width and height of the ridge. Together, we propose a smart method to change the surface strain field and provide a simple, yet effective, high-throughput, programmable pneumatically actuated multifunctional stretching chip.

2. Materials and Methods

2.1. Fabrication of Cell Stretching Chip

The cell stretching chip was composed of three layers, including the top elastic membrane layer with a periodic ridge structure, the middle pressure control layer with a circle cavity array, and the bottom glass substrate (Figure S1). The cell stretching chip was fabricated using the standard soft-lithography technique [28–30]. Briefly, in order to fabricate the periodic ridge structure, a photomask was printed according to the designed pattern, and the ridge template was fabricated by the spin-coating SU8-3025 photoresistor (Microchem, Newton, MA, USA) on a silicon wafer at 2000 rpm for 45 s. After silylanization, the wafer was coated with a thin layer of a PDMS prepolymer containing the base monomers and cuing agents (10:1 *w*/*w*; Sylgard 184, Dow-Corning, Bay City, MI, USA) using a spin coater; the thickness of PDMS layer was precisely controlled by the spin speed. Then, the elastic membrane with a periodic ridge structure was cured at 100 °C for 1 h. Similarly, the pressure control layer was also fabricated in the same way. Chip assembly was achieved by step-by-step plasma bonding while employing the alignment platform (WH-AM-01, Wenhao Co., Ltd., Suzhou, China) to ensure one of the ridges crossing the center of the cavities. Then, a cylinder halo (Diameter: 20 mm, Height: 10 mm) was plasma bonded on the elastic membrane, which acted as a culture dish to support a long-term cell culture.

Finally, a cell stretching chip 75 mm in length, 25 mm in width, and 13 mm in height was fabricated and sterilized by UV and then coated with collagen I (C8060, Solarbio, Beijing, China) for the cell culture.

2.2. Characterization of Pressure Control Layer

Membrane thickness measurement: The PDMS membrane thickness, which is mainly decided by the spin speed, affects the ridge's stretch strain greatly. The thickness was measured by the surface profiler (Alpha-step IQ, KLA-Tencor, Milpitas, CA, USA).

2.3. FEM Simulation and Experimental Measurement for Strain

In order to determine the strain field distribution in the cell stretching chip, both FEM simulation and experimental validation were used to measure the strain in the surface ridge structure. Briefly, FEM simulation based on an incompressible hyper-elastic (neo-Hookean) model was performed to calculate the displacement and strain field of the top elastic membrane. Young's modulus of the PDMS elastic membrane was ~3.7 MPa measured by AFM (MFP-3D, Asylum Research, Santa Barbara, CA, USA).

To validate the simulation results, the strain field distribution was further measured by the experimental method. We prepared a circular fluorescent dot array on the surface of the ridge using microcontact printing. When the cell stretching chip was subjected to a positive pressure, the circular dot deformed according to the stretching. The strains in the longitudinal and lateral directions were measured by the change in diameter between the relaxed and stretching states in the corresponding direction.

2.4. Cell Culture and Stretching

A549 cell was maintained in RPMI-1640 medium (Thermo Fisher Scientific, Waltham, MA, USA) supplemented with 10% (v/v) fetal bovine serum (FBS, Gibco, Melbourne, Australia) and 100 U/mL penicillin–streptomycin Thermo Fisher Scientific, in a 5% CO_2 incubator at 37 °C. A549 was seeded in the cell stretching chip at a density of 2×10^5 per chip. Four hours after seeding to allow cells to adhere and spread, the square pulse signal was imputed by a multichannel pressure controller (OB1 MK3+, Elveflow, Paris, France) to stretch the cells. Parameters of the stretching stimulation, such as pressure amplitude, frequency and duty ratio, could be easily set in the software of the pressure controller.

2.5. Cytoskeleton Staining

Cells were fixed with 4% paraformaldehyde for 30 min at room temperature and then permeabilized with 0.3% Triton X-100 in PBS for 5 min. Subsequently, the cells were stained with DAPI, phalloidin Thermo Fisher Scientific, and anti-vinculin antibody. Fluorescence images were taken using a Nikon confocal microscope with a 40× water immersion objective.

2.6. Measurement of Cell Orientation Index

To quantify the orientation of the cells cultured on the ridge surface of a stretching chip, we established a coordinate system with the lateral axial (x axial) parallel to the width of the ridge and longitudinal axial (y axial) parallel to the length of the ridge. The cells were fit with ellipses by ImageJ software, and the orientation angle (θ) between the long axis of the cells and the lateral axis of the defined coordinate system was measured. To simplify the statistics, the orientation angle was processed ranging from 0° to 90°. Then, the cell orientation index (γ_c) was further calculated to reflect the cell arrangement using the formula as follows:

$$\gamma_c = \sum_{i=1} (cos\theta_i - sin\theta_i) P_i \quad (1)$$

where i (i_{max} = 9) and P_i were the divided angle group number per 10° and the percentage of the orientation angle distribution, respectively.

This is a measure of the orientation of the cells centered around zero: positive and negative values indicate the orientation in the longitudinal and lateral directions, respectively, and the magnitude indicates the extent of the orientation in the given direction.

2.7. Statistical Analysis

All error bars were shown as the mean ± standard deviations from the experiments that were performed in at least three independent experiments. Statistical analysis was analyzed with one-way analysis of variance (ANOVA) followed by Tukey's test using GraphPad Prism software (https://www.graphpad.com). Statistical significance was accepted when the *p*-value was less than 0.05 for all indicated comparisons.

3. Results and Discussion

In our present work, inspired by the topological defects principle in solid mechanics, we introduce a ridge structure in a traditional pneumatically actuated balloon-like device to change the membrane surface strain field (Figure 1A). We incorporated a ridge structure into the pneumatic cavity stretching membrane (Figure S1). From the 3D top view image, one can see that the ridge was stretched along the longitudinal direction because of the structure confinement (Figure 1A). In conjunction with microfluidic technology, our ridge structure-dictated cell stretching chip consisted of three layers, i.e., an elastic membrane layer, a pressure control layer, and a glass substrate (Figure 1B). The periodic ridges of the rectangle cross-section were assembled on the surface of the elastic membrane layer (Figure 1B).

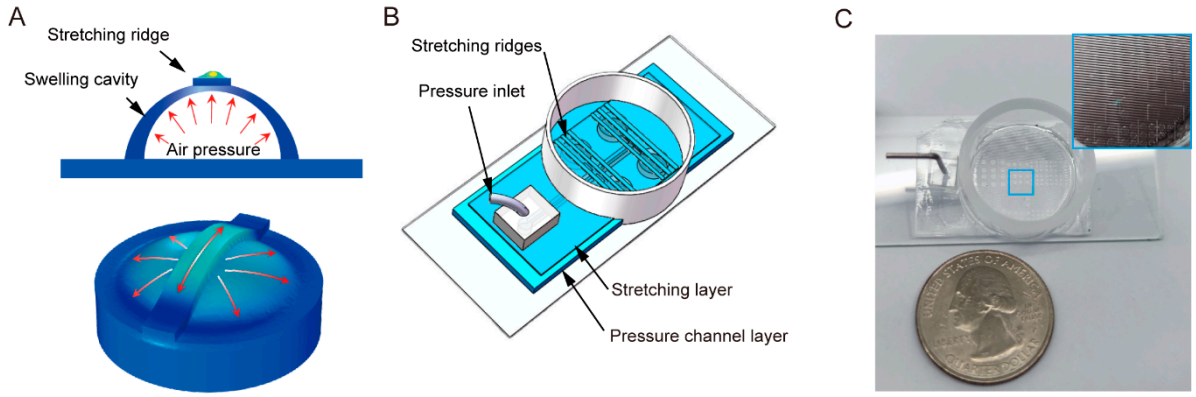

Figure 1. Ridge surface-dictated cell stretching chip. (**A**) Concept of cell stretching chip. Up panel is a cross-sectional view of the stretched cavity under air pressure. Down panel is a 3D view of the stretched ridge on the surface of the elastic stretching layer. (**B**) Schematic and (**C**) physical pictures of the stretching device. The stretching chip consists of three layers, i.e., top elastic membrane layer with a periodic ridge structure, middle pressure control layer with a circle cavity array, and a bottom glass substrate.

To validate the stretching mode of our cell stretching chip, experiment measurements and FEM simulation analysis were conducted to analyze the strain field on the surface of the ridge structure. To take a side view of the expansion process of the cavities, our chip was firstly placed vertically on the stage of microscopy; then, the cavities that were on the edge of the chip were focused accurately on the equatorial plane. In one inflation cycle, a high-speed CCD camera (Mikrotron, EoSens CL, Landshuter, Germany) installed during microscopy (CKX41, OLYMPUS, Tokyo, Japan) was used to capture the stretching process in a cross-sectional view. We first stretched the ridges with 100-μm width and 50-μm height under the pressure of 1 bar, and the frequency of 1 Hz with a duty ratio of 0.5 (Figure 2A). One could clearly see a dynamic stretching process, as the membrane gradually expanded within the stretch period, with the maximum stretch at 0.5 s. We further measured the normal displacement of the cavity along the diameter from the cross-sectional view image

at 0.5 s (Figure 2A). The height displacement of the selected region of interest (ROI, see the points in Figure 2A) under 1 bar (red points) represented a parabolic distribution with the center as symmetrical point (Figure 2B), which was consistent with previous studies [15]. We also measured the height displacement under the conditions of 0.8 and 0.5 bar, and the experiment measured data (Exp. Data) perfectly fit with the displacement curve calculated by the simulation model, demonstrating the accuracy of our simulation model. Based on the simulation results, strain distribution along the ridge structure could also be obtained. We plotted the longitudinal strain distribution (longitudinal of ridge) on the stretched ridges at different pressures (Figure 2C). The value of the strain varied from 8% to 15%, with the pressure increasing from 0.5 to 1 bar, meeting the strain range requirement for the cell stretching assay [15]. Moreover, take the cavity with a diameter of 800 µm as an example, the strain value remained constant in most areas of the ridge from 180 to 620 µm (Figure 2C), showing a stable stretching mode.

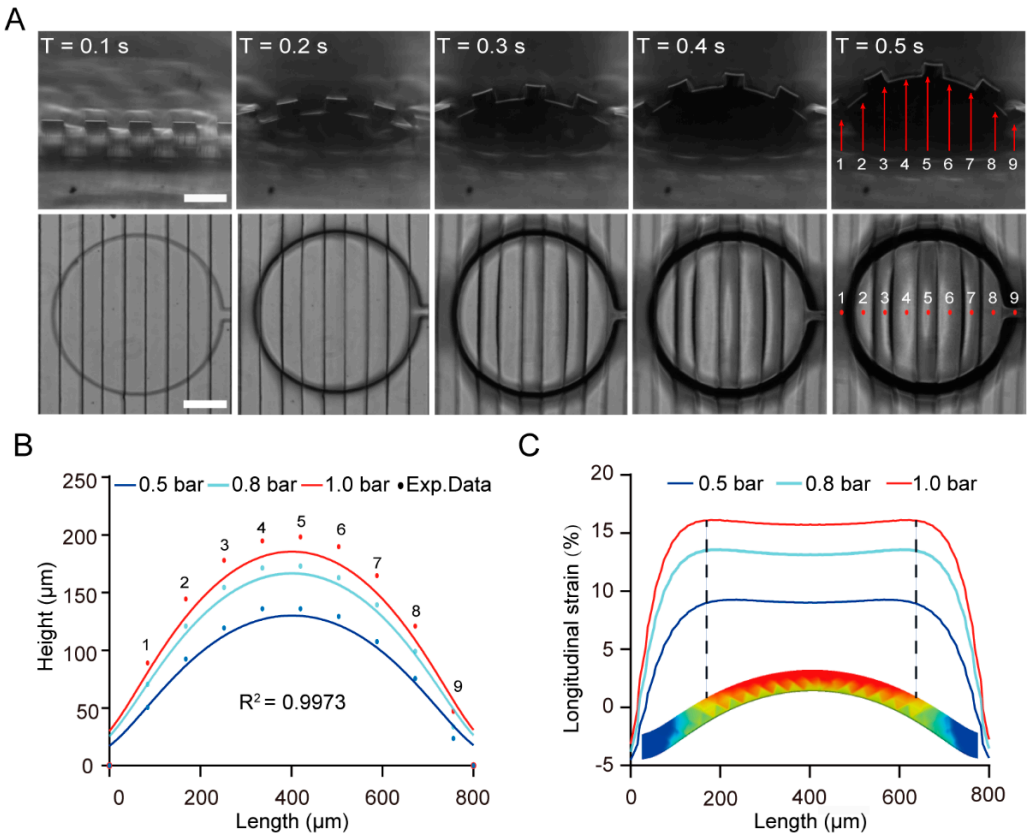

Figure 2. The pneumatically actuated membrane deformation and simulation results of a strain in the ridge structure. (**A**) Pneumatic stretching process of the stretching chip. Images showing the cross-sectional (up panel) and top (down panel) views of one swelling cavity deformation in one inflation cycle under a given pressure (ΔP = 1 bar) of 1 Hz. Scale bar: 200 µm. (**B**) Quantitative data showing the maximum height of membrane expansion deformation under the indicated pressure corresponding to the measurement points selected in (**A**). Lines represent the simulation results, and dots show the experimental measurements. (**C**) Plot of the longitudinal strain distribution on a stretched ridge under the indicated pressure conditions. The diameter of the pressure cavity is 800 µm. The width of ridge is 100 µm.

In contrast to the equiaxial strain field on the traditional flat surface, it is obvious that the ridge was stretched in the longitudinal direction and squeezed in the lateral direction (Figure 3A). This difference between lateral and longitudinal strain was consistent with the property of a typical uniaxial stretch strain distribution [3,31], demonstrating that the ridge structure can easily change the equiaxial strain to a uniaxial strain manner instead of

changing the working mode of the actuator, such as in traditional strategy [3]. The change of the stretch mode was mainly affected by the surface topography. To further validate this uniaxial stretch mode, we measured the deformation of the circular fluorescent dots on the ridge (Figure 3B). It is apparent that the circle became an ellipse under stretching. The dots were stretched longer, around 10% in the longitudinal direction, and shrunk simultaneously about 5% in the lateral direction (Figure 3C), which could be ascribed to the Poisson's effect on elastic materials. Through a statistical analysis by SPSS, the *p*-value was 0.900, demonstrating that the experimental results were consistent with the simulation results (Figure 3C). In conjunction with the advantages of the microfluidic platform [25], our surface ridge structure-dictated cell stretching chip makes it easy to achieve the high-throughput test by creating a cavity array, such as 1000 units (column × row: 10 × 100) (data not shown here).

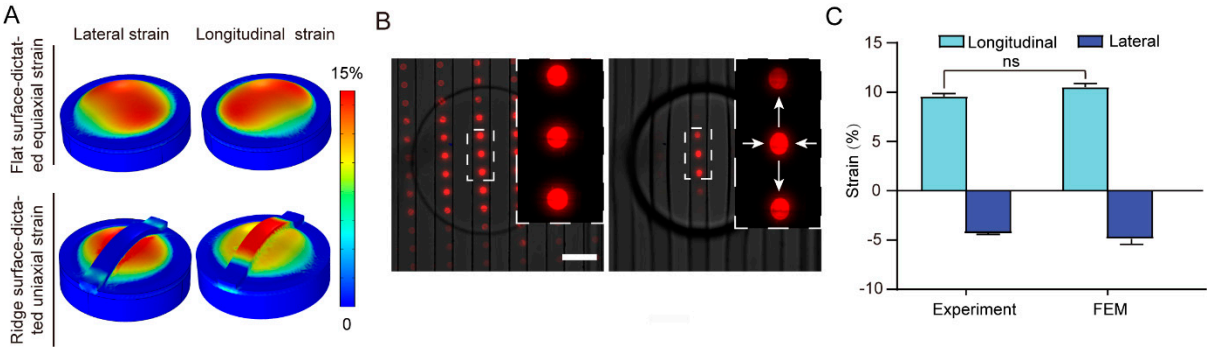

Figure 3. Characterization of the uniaxial strain property of the stretching chip. (**A**) Lateral and longitudinal strain field distribution of the pressure cavity with a flat surface (up panel) and ridge structure (down panel) based on FEM. (**B**) Representative phase and fluorescence images showing the deformation of the pressure cavity and fluorescent dots under 0 bar pressure (left panel) and 0.5 bar pressure (right panel), respectively. Scale bar: 200 μm. (**C**) Quantitative data showing the lateral and longitudinal strain from experimental and FEM simulation assays ($p = 0.100$, ns).

In order to further analyze the performance and scalability of our stretching chip, we measured the strain value and distribution of all the ridges on one cavity more carefully based on the simulation (Figure 4A and Figure S2). It is evident that the uniaxial stretching mode was present on all the ridges. We acquired the strain value of the ROIs on the ridges (Figure 4B, see the indicated edge and center ROIs). We found that the strain increased from 8% on the ridge located at the edge of the cavity to 15% on the ridge located at the center of the cavity under one pressure condition. Meanwhile, the strain value could also be adjusted from 5% to 15%, with the cavity's diameter increasing from 500 to 1000 μm (data not shown here). These all are beneficial to improve the throughput and simplify the experimental system. The decrease of the strain on the edge of the cavity could be ascribed to the circle border constraint. We further investigated the effect of the ridge's width on the strain field manner. Our results showed that the uniaxial strain pattern appeared on the ridge of each width (50, 100, and 150 μm), representing ridge width independent fashion. Meanwhile, the longitudinal strain values were also similar to the ridge with different widths.

Together, by means of our creative design, we bridged the gap between the traditional pneumatic stretching technique and well-accepted uniaxial stretch application, which was crucially important for promoting the integrated research of mechanical stimulation in vitro [1]. Previous researchers have demonstrated that the cellular response to a strain stimulation is strain value-dependent [3,32]. This requests high experiment standards that eliminate the groups' deviation and increases the throughput, which is difficult to achieve based on the traditional method due to the limitation of the stretching mechanism. Besides the high-throughput, the realization of the strain gradient on our stretching chip also facilitated the research strategy. Another advantage of our stretching chip that deserves being emphasized is the potential programmable design of the strain field through

modulating the parameters of the ridge, including the width and height (Figure S3). The strain field is commonly regulated by the cooperation of actuating motors in different directions or adding a supply of air pressure and control channels based on the current stretching methods [33]. Better than these strategies, we can easily program the distribution of the strain field, including the equiaxial strain, uniaxial strain, and biaxial strain, by purposefully designing the topography on the elastic stretching membrane. Based on the cooperative property, topography structure with various structure feature sizes could also be designed on purpose so that different modes of a stretch stimulation could be applied simultaneously on this novel cell stretching chip. It provided potential for the application in some areas, such as cell interaction and tissue engineering [9,34].

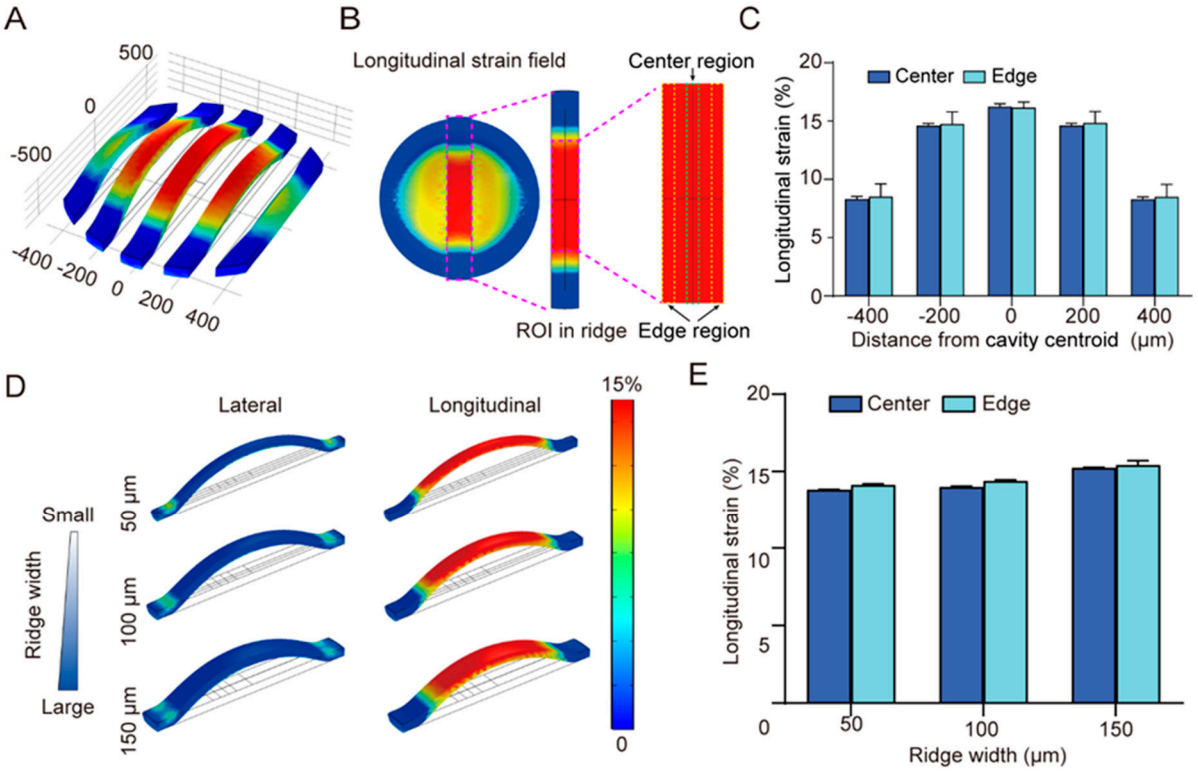

Figure 4. Uniaxial strain property is independent of the ridge location in a pressure cavity and the ridge width. (**A**) Longitudinal strain field distribution in all of the ridges within one pressure cavity. The diameter of the pressure cavity is 1000 μm. The width of ridge is 100 μm. (**B**) Center and edge regions of interest (ROIs) in a ridge represent the regions that were used for analyzing the longitudinal strain. (**C**) Bar plot showing the longitudinal strain of the center and edge regions in the ridge indicated in (**A**). (**D**) Lateral and longitudinal strain field distributions in a ridge with a width of 50, 100, and 150 μm under 0.8 bar pressure. (**E**) Bar plot showing the quantitative data of the longitudinal strain of the center and edge regions (indicated in **A**) in a ridge with different widths.

Cells in the body were continuously subjected to mechanical strains and respond through both morphology and biochemical changes. Among these cells, lung alveolar epithelial cells experience a cyclic linear stretch strain (5~15%) at a frequency of 0.2~0.3 Hz under normal conditions. However, the amplitude and frequency of the cyclic strain differ significantly under pathological conditions. For example, some patients' breath frequencies increased up to about 50 times per minute when suffering from acute respiratory distress syndrome. When the cells were subjected to a cyclic stretching stimulation in vitro, the change occurred gradually and achieved a stable situation, indicating that the cells were able to adjust to the cyclic stretching stimulation to maintain the biomechanical homeostasis. To demonstrate the potential of our cell stretching chip, cells cultured on the chip were stretched under a series of stretch situations and analyzed for cell orientation (Figure 5A).

Our results showed that the orientation of A549 cells, a human alveolar basal epithelial cancer cell line, which is often chosen as a study model to investigate lung-relevant diseases, was clearly parallel to the lateral direction of the ridge after stretching for 24 h, further demonstrating the uniaxial strain manner of our stretching chip. The same results could also be observed on the orientation of the cell nucleus and F-actin fiber (Figure 5B), which is consistent with previous studies [3,35], suggesting that the cells readjusted their contractile activity and reoriented their cytoskeleton to achieve stable conditions in response to the stretching stimulation.

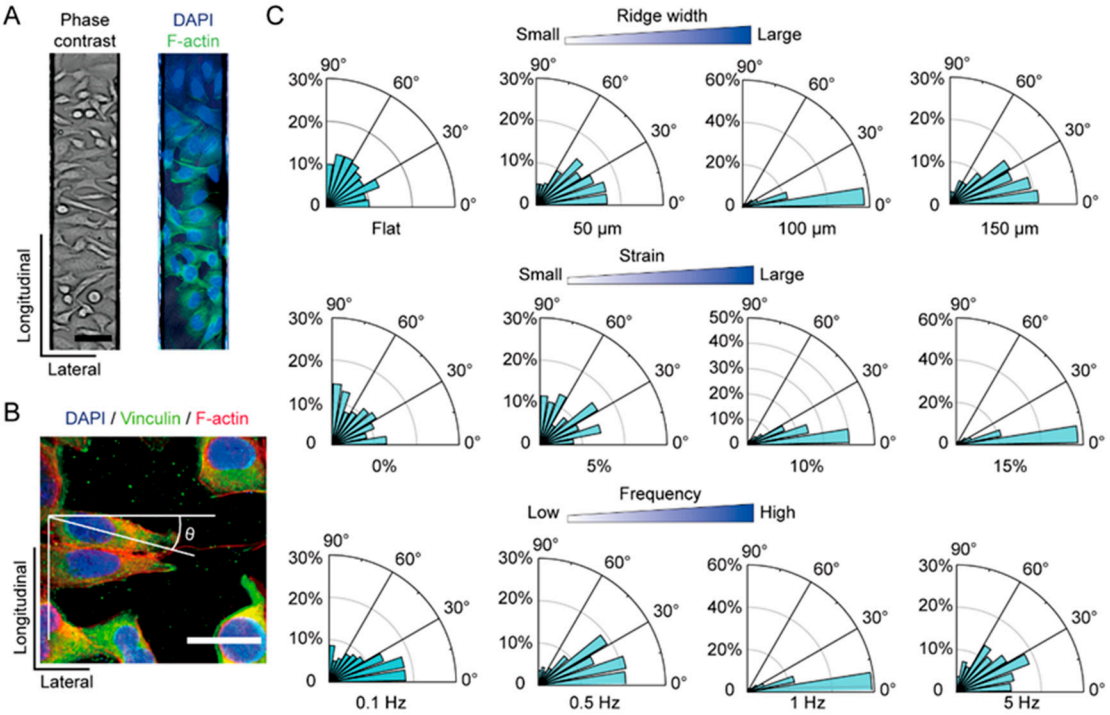

Figure 5. Cell orientation reflected the uniaxial strain feature of the stretching chip. (**A**) Representative phase contrast (left) and fluorescent (right) images of A549 cells cultured on a ridge surface of the stretching chip after being stretched at 1 bar for 24 h. Scale bar: 50 μm. (**B**) Illustration of the cell orientation angle measurement. Scale bar: 50 μm. (**C**) Angular distributions of the cell orientation of A549 cells under the indicated ridge width (top panel), strain (middle panel), and stretching frequency (down panel) conditions.

To further quantify the cell orientation, we measured the angle θ between the lateral direction and long axial direction of the cell as the orientation feature. When the cells were adhered on a flat surface, the cells did not prefer to orient in any direction (Figure 5C) due to the cyclic equiaxial stretch [36,37]. Cells gradually aligned at 0 degree when the width of the ridge was 50, 100, and 150 μm. As for the strain, when the strain was less than 5%, the cells did not present obvious orientation behavior, while, when the strain was greater than 10%, the cells aligned at 0 degree (Figure 5C), showing strain-dependent behavior, which was consistent with previous studies that cellular stress fiber (SF) reorganization is dependent on the stretching strain value [36]. Except the ridge width and strain ratio, the dynamic features such as pressure signal frequency also contributed to the cell arrangement in response to stretching [34]. Below 1 Hz, the degree of cell orientation was pertinent to the frequency. At 5 Hz, the cell orientation behavior decreased (Figure 5C). This tendency could be ascribed to the dynamic stochastic model about rate-dependent SF reorganization induced by matrix stretching [36]. In this model, when the stretching rate was faster than the SF self-adjustment, the SF would disassemble and gradually accumulate in the direction of the smallest perturbation. Furthermore, the index of cell orientation, γ_c, was defined

to evaluate the extent of the cell orientation (Figure 6). Together, these results of the cell orientation demonstrated the uniaxial stretching mode of our chip.

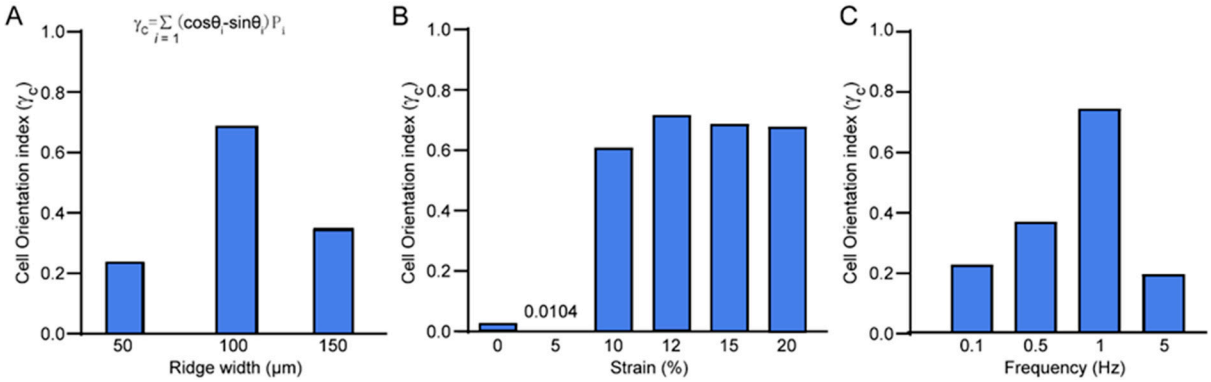

Figure 6. Cell orientation index showing the relationship between the cell arrangement and ridge width (**A**), strain (**B**), and stretching frequency (**C**). When the index is near 0, the cells are oriented randomly. When the index is near 1, the cells are parallel to the lateral direction. If the index is near −1, the cells are orientated in the longitudinal direction.

4. Conclusions

In conclusion, our work proposed a new device of introducing a ridge structure to modulate the strain manner and fabricated a new chip through making a ridge structure on the pneumatically actuated balloon-like device to produce a uniaxial strain. Together, the developed design successfully provided a new high-throughput method in the investigation of the mechanical stimulation, which could enrich the application of pneumatically actuated stretching and also provide new potential for further applications in mechanobiology.

Supplementary Materials: The following supporting information can be downloaded at https://www.mdpi.com/article/10.3390/chemosensors10080302/s1. Figure S1: Fabrication process and assembly strategy of the stretching chip. Figure S2: Lateral strain distribution on multi stretched ridges. Figure S3: Structure feature sizes of the ridge-regulated strain.

Author Contributions: Conceptualization, C.X. and X.F.; methodology, X.F.; validation, X.F. and P.W.; writing—original draft preparation, X.F.; writing—review and editing, F.L., J.H., J.F. and C.X.; supervision, C.X. and F.L.; project administration, C.X. and funding acquisition, C.X., F.L. and J.F. All authors have read and agreed to the published version of the manuscript.

Funding: This work was supported in part by the National Natural Science Foundation of China (NSFC) under grant No. 12072001 to J.F., 11902007 to F.L., and 11972002 to C.X.

Institutional Review Board Statement: Not applicable.

Informed Consent Statement: Not applicable.

Data Availability Statement: Not applicable.

Conflicts of Interest: The authors declare no conflict of interest.

References

1. Kamble, H.; Barton, M.J.; Jun, M.; Park, S.; Nguyen, N.T. Cell stretching devices as research tools: Engineering and biological considerations. *Lab Chip* **2016**, *16*, 3193–3203. [CrossRef] [PubMed]
2. Riehl, B.D.; Park, J.H.; Kwon, I.K.; Lim, J.Y. Mechanical stretching for tissue engineering: Two-dimensional and three-dimensional constructs. *Tissue Eng. Part B Rev.* **2012**, *18*, 288–300. [CrossRef] [PubMed]
3. Cui, Y.; Hameed, F.M.; Yang, B.; Lee, K.; Pan, C.Q.; Park, S.; Sheetz, M. Cyclic stretching of soft substrates induces spreading and growth. *Nat. Commun.* **2015**, *6*, 6333. [CrossRef] [PubMed]
4. Ghibaudo, M.; Trichet, L.; Le Digabel, J.; Richert, A.; Hersen, P.; Ladoux, B. Substrate topography induces a crossover from 2D to 3D behavior in fibroblast migration. *Biophys. J.* **2009**, *97*, 357–368. [CrossRef] [PubMed]
5. Heo, S.J.; Driscoll, T.P.; Thorpe, S.D.; Nerurkar, N.L.; Baker, B.M.; Yang, M.T.; Chen, C.S.; Lee, D.A.; Mauck, R.L. Differentiation alters stem cell nuclear architecture, mechanics, and mechano-sensitivity. *eLife* **2016**, *5*, e18207. [CrossRef]

6. Kong, M.; Lee, J.; Yazdi, I.K.; Miri, A.K.; Lin, Y.D.; Seo, J.; Zhang, Y.S.; Khademhosseini, A.; Shin, S.R. Cardiac Fibrotic Remodeling on a Chip with Dynamic Mechanical Stimulation. *Adv. Healthc. Mater.* **2019**, *8*, e1801146. [CrossRef]
7. Boudou, T.; Andersen, T.; Balland, M. On the spatiotemporal regulation of cell tensional state. *Exp. Cell Res.* **2019**, *378*, 113–117. [CrossRef] [PubMed]
8. Zhang, W.; Huang, G.; Xu, F. Engineering Biomaterials and Approaches for Mechanical Stretching of Cells in Three Dimensions. *Front. Bioeng. Biotechnol.* **2020**, *8*, 589590. [CrossRef]
9. Costa, J.; Ahluwalia, A. Advances and Current Challenges in Intestinal in vitro Model Engineering: A Digest. *Front. Bioeng. Biotechnol.* **2019**, *7*, 144. [CrossRef]
10. Guenat, O.T.; Berthiaume, F. Incorporating mechanical strain in organs-on-a-chip: Lung and skin. *Biomicrofluidics* **2018**, *12*, 042207. [CrossRef]
11. Zheng, W.; Jiang, B.; Wang, D.; Zhang, W.; Wang, Z.; Jiang, X. A microfluidic flow-stretch chip for investigating blood vessel biomechanics. *Lab Chip* **2012**, *12*, 3441–3450. [CrossRef] [PubMed]
12. Sunuwar, L.; Yin, J.; Kasendra, M.; Karalis, K.; Kaper, J.; Fleckenstein, J.; Donowitz, M. Mechanical Stimuli Affect Escherichia coli Heat-Stable Enterotoxin-Cyclic GMP Signaling in a Human Enteroid Intestine-Chip Model. *Infect. Immun.* **2020**, *88*, e00866-19. [CrossRef] [PubMed]
13. Li, J.; Wang, Z.; Chu, Q.; Jiang, K.; Li, J.; Tang, N. The Strength of Mechanical Forces Determines the Differentiation of Alveolar Epithelial Cells. *Dev. Cell* **2018**, *44*, 297–312. [CrossRef] [PubMed]
14. Wu, H.; Yu, Y.; Huang, H.; Hu, Y.; Fu, S.; Wang, Z.; Shi, M.; Zhao, X.; Yuan, J.; Li, J.; et al. Progressive Pulmonary Fibrosis Is Caused by Elevated Mechanical Tension on Alveolar Stem Cells. *Cell* **2020**, *180*, 107–121. [CrossRef]
15. Michielin, F.; Serena, E.; Pavan, P.; Elvassore, N. Microfluidic-assisted cyclic mechanical stimulation affects cellular membrane integrity in a human muscular dystrophy in vitro model. *RSC Adv.* **2015**, *5*, 98429–98439. [CrossRef]
16. Dolle, J.P.; Morrison, B.; Schloss, R.S.; Yarmush, M.L. An organotypic uniaxial strain model using microfluidics. *Lab Chip* **2013**, *13*, 432–442. [CrossRef] [PubMed]
17. Gaio, N.; van Meer, B.; Quiros Solano, W.; Bergers, L.; van de Stolpe, A.; Mummery, C.; Sarro, P.M.; Dekker, R. Cytostretch, an Organ-on-Chip Platform. *Micromachines* **2016**, *7*, 120. [CrossRef]
18. Schurmann, S.; Wagner, S.; Herlitze, S.; Fischer, C.; Gumbrecht, S.; Wirth-Hucking, A.; Prolss, G.; Lautscham, L.A.; Fabry, B.; Goldmann, W.H.; et al. The IsoStretcher: An isotropic cell stretch device to study mechanical biosensor pathways in living cells. *Biosens. Bioelectron.* **2016**, *81*, 363–372. [CrossRef]
19. Seriani, S.; Del Favero, G.; Mahaffey, J.; Marko, D.; Gallina, P.; Long, C.S.; Mestroni, L.; Sbaizero, O. The cell-stretcher: A novel device for the mechanical stimulation of cell populations. *Rev. Sci. Instrum.* **2016**, *87*, 084301. [CrossRef] [PubMed]
20. Kamble, H.; Barton, M.J.; Nguyen, N.-T. Modelling of an uniaxial single-sided magnetically actuated cell-stretching device. *Sens. Actuators A Phys.* **2016**, *252*, 174–179. [CrossRef]
21. Kamble, H.; Vadivelu, R.; Barton, M.; Boriachek, K.; Munaz, A.; Park, S.; Shiddiky, M.J.A.; Nguyen, N.T. An Electromagnetically Actuated Double-Sided Cell-Stretching Device for Mechanobiology Research. *Micromachines* **2017**, *8*, 256. [CrossRef] [PubMed]
22. He, Y.; Mao, T.; Gu, Y.; Yang, Y.; Ding, J. A simplified yet enhanced and versatile microfluidic platform for cyclic cell stretching on an elastic polymer. *Biofabrication* **2020**, *12*, 045032. [CrossRef] [PubMed]
23. Kamble, H.; Vadivelu, R.; Barton, M.; Shiddiky, M.J.A.; Nguyen, N.T. Pneumatically actuated cell-stretching array platform for engineering cell patterns in vitro. *Lab Chip* **2018**, *18*, 765–774. [CrossRef] [PubMed]
24. Ao, M.; Brewer, B.M.; Yang, L.; Franco Coronel, O.E.; Hayward, S.W.; Webb, D.J.; Li, D. Stretching fibroblasts remodels fibronectin and alters cancer cell migration. *Sci. Rep.* **2015**, *5*, 8334. [CrossRef] [PubMed]
25. Prevedello, L.; Michielin, F.; Balcon, M.; Savio, E.; Pavan, P.; Elvassore, N. A Novel Microfluidic Platform for Biomechano-Stimulations on a Chip. *Ann. Biomed. Eng.* **2019**, *47*, 231–242. [CrossRef] [PubMed]
26. Walker, M.; Godin, M.; Pelling, A.E. A vacuum-actuated microtissue stretcher for long-term exposure to oscillatory strain within a 3D matrix. *Biomed. Microdevices* **2018**, *20*, 43. [CrossRef]
27. Xue, X.; Sun, Y.; Resto-Irizarry, A.M.; Yuan, Y.; Aw Yong, K.M.; Zheng, Y.; Weng, S.; Shao, Y.; Chai, Y.; Studer, L.; et al. Mechanics-guided embryonic patterning of neuroectoderm tissue from human pluripotent stem cells. *Nat. Mater.* **2018**, *17*, 633–641. [CrossRef]
28. Chen, K.; Rong, N.; Wang, S.; Luo, C. Corrigendum to: A novel two-layer-integrated microfluidic device for high-throughput yeast proteomic dynamics analysis at the single-cell level. *Integr. Biol.* **2021**, *13*, 258. [CrossRef]
29. Li, X.; Shi, J.; Gao, Z.; Xu, J.; Wang, S.; Li, X.; Ouyang, Q.; Luo, C. Biophysical studies of cancer cells' traverse-vessel behaviors under different pressures revealed cells' motion state transition. *Sci. Rep.* **2022**, *12*, 7392. [CrossRef] [PubMed]
30. Zhang, J.; Shen, W.; Cai, Z.; Chen, K.; Ouyang, Q.; Wei, P.; Yang, W.; Luo, C. Microfluidic-Enabled Multi-Cell-Densities-Patterning and Culture Device for Characterization of Yeast Strains' Growth Rates under Mating Pheromone. *Chemosensors* **2022**, *10*, 141. [CrossRef]
31. Sorba, F.; Poulin, A.; Ischer, R.; Shea, H.; Martin-Olmos, C. Integrated elastomer-based device for measuring the mechanics of adherent cell monolayers. *Lab Chip* **2019**, *19*, 2138–2146. [CrossRef] [PubMed]
32. Li, X.; Chu, J.; Wang, A.; Zhu, Y.; Chu, W.K.; Yang, L.; Li, S. Uniaxial mechanical strain modulates the differentiation of neural crest stem cells into smooth muscle lineage on micropatterned surfaces. *PLoS ONE* **2011**, *6*, e26029. [CrossRef] [PubMed]

33. Chagnon-Lessard, S.; Godin, M.; Pelling, A.E. Time dependence of cellular responses to dynamic and complex strain fields. *Integr. Biol.* **2019**, *11*, 4–15. [CrossRef] [PubMed]
34. Esfahani, A.M.; Rosenbohm, J.; Safa, B.T.; Lavrik, N.V.; Minnick, G.; Zhou, Q.; Kong, F.; Jin, X.; Kim, E.; Liu, Y.; et al. Characterization of the strain-rate-dependent mechanical response of single cell-cell junctions. *Proc. Natl. Acad. Sci. USA* **2021**, *118*, e2019347118. [CrossRef]
35. Su, W.T.; Liao, Y.F.; Chu, I.M. Observation of fibroblast motility on a micro-grooved hydrophobic elastomer substrate with different geometric characteristics. *Micron* **2007**, *38*, 278–285. [CrossRef] [PubMed]
36. Hsu, H.J.; Lee, C.F.; Kaunas, R. A dynamic stochastic model of frequency-dependent stress fiber alignment induced by cyclic stretch. *PLoS ONE* **2009**, *4*, e4853. [CrossRef]
37. Kaunas, R.; Usami, S.; Chien, S. Regulation of stretch-induced JNK activation by stress fiber orientation. *Cell. Signal.* **2006**, *18*, 1924–1931. [CrossRef]